A Mm-wave Ultra-Long-Range Energy-Autonomous Printed RFID-enabled Van-Atta Wireless Sensor: at the Crossroads of 5G and IoT

Jimmy G.D. Hester, and Manos M. Tentzeris
Department of Electrical and Computer Engineering, Georgia Institute of Technology,
Atlanta, GA, 30332 USA e-mail: jimmy.hester@gatech.edu

***Abstract*—In this paper the authors report the first 5G-compatible implementation of a long-range, energy-autonomous, mm-wave RFID sensor for IoT applications. The system topology is first described, before the design and performance characterization of its constituting components, including an inkjet-printed carbon-nanotube(CNT)-based ammonia sensor, are presented. Then, the entire printed mm-wave backscatter-modulation device is tested, demonstrating a monostatic cross-polarized radar cross-section of $-29\,\mathrm{dBsm}$, with only a $10\,\mathrm{dB}$ variation within the -50° to 50° interrogation angular range. The wireless ammonia sensing capabilities of the system are then demonstrated, before its detection at an ultra-long-range of $80\,\mathrm{m}$ is reported.**

***Index Terms*—5G, internet of things, wireless sensing, inkjet-printing, RFID**

I. Introduction

Radio Frequency IDentification (RFID) devices have become pervasive in the modern world. Passive RFIDs, as opposed to their active or semi-passive counterparts, have witnessed the widest adoption, as a consequence of their low cost, enabled by their minimalist architectures and battery-free energy autonomy. Current research trends have striven towards extending the performance of RFID architectures, and enabling them with additional capabilities, such as sensing. These efforts are generally driven by the appeal–in the context of the Internet of Things (IoT)– towards compact devices capable of connecting large numbers of common yet smart objects, in a cost efficient manner. The archetype of functional IoT nodes, for instance, is the concept of the Smart Skin: a connected smart surface that can sense and react to its environment. Nevertheless, the main advantage of passive RFIDs (their lack of need for a battery) is also the source of their main weakness: a short interrogation range (generally less than $10\,\mathrm{m}$), that tremendously decreases when sensing capabilities are added to the device [1]. In typical implementations, this is the result of the combination of the low maximum allowed power in the UHF band, and the need for RF energy harvesting. Nevertheless, even if the hindrance of RF energy harvesting is removed, through the use of solar energy harvesting [2], for instance, low power limitations at UHF still significantly limit the reading range. With this in mind, it is possible to recognize, in the rising field of mm-wave RF electronics and 5G technologies, a wide landscape of opportunities for RFID IoT devices. Indeed, as already demonstrated for chipless RFIDs [3] and enabled by the remarkable combination of high and near-isotropic radar cross section (RCS) of the Van-Atta reflectarray structure [4], the rise to mm-wave frequencies operation–compounded with the far less stringent limitations on maximum emitted power–can bring with it large performance advantages. Furthermore, this frequency band opens up the near-direct interfacing of RFIDs with explosively-growing 5G systems and networks. As such, an RFID device, capable of operating autonomously at mm-wave, and with a reading range of several tens or hundreds of meters would provide a very effective interface point between the IoT (including Smart Skins) and 5G networks. The goal of the work reported in this paper is to demonstrate the first implementation of such a device. In this effort, the authors report the first (to their knowledge) implementation of a long-range, energy autonomous, mm-wave RFID sensor, in the shape of a solar-powered amplitude-modulating backscattering $28\,\mathrm{GHz}$ cross-polarizing Van-Atta wireless sensor structure. In Sec. II, a description of the overall system, along with several defining metrics of mm-wave operation, are provided. Then, in Sec. III, a description of the design process and measured performance of the individual components of the RFID system are given, before testing and measured performance of the entire wireless sensor are discussed in Sec. IV. Finally, a conclusion is drawn in Sec. V.

II. Printed mm-wave RFID system description

Essential elements of RFID systems include an antenna, a backscatter-modulation front-end, modulation logic, and an energy source. In the context of ubiquitous components for the IoT, four main requirements guide systems design: low cost, energy autonomy, flexibility, and low environmental footprint fabrication and life cycle. In order to provide an optimal solution, the proposed system was designed based on a minimalist oscillator-based continuous-wave (CW) amplitude modulation backscatter communications approach, using single-transistor switches and a low power oscillator. With this scheme, several tags can be identified by their specific backscatter-modulation frequency or frequency range. This minimalist design also allowed the full powering of the system with a compact, flexible solar cell. Furthermore, the environmentally-friendly and flexible-substrate-compatible inkjet-printing method was utilized to fabricate the passive elements and traces of the circuit, as well as a fully-printed CNT-based ammonia sensor. Finally, these components were integrated, at the $28\,\mathrm{GHz}$ 5G band, around a Van-Atta reflectarray structure whose remarkable properties–already enabling high performance passive mm-wave chipless RFID structures [3]–provide a high and near-isotropic radar cross section (or, equivalently, detectability).

978-1-5090-6360-4/17/$31.00 ©2017 IEEE

III. Components of the System

A. Low-cost mm-wave switch for backscatter-modulation

For the implementation of the mm-wave switch for backscatter-modulation, the minimalist design shown on the inset of Fig. 1 was adopted. The structure is built around a low cost mm-wave-compatible transistor (NE3520S03), and essentially operates by switching the length of a parallel stub from $\frac{\lambda}{4}$ to $\frac{\lambda}{2}$. After design, the structure was inkjet-printed with a Dimatix DMP2830 using silver nanoparticle (SNP) ink from Suntronic on Rogers 3850HT LCP substrate (this substrate is used for all subsequently presented devices, and for the overall system), and measured with an Anritsu 37369A VNA. The S-parameters values, with the feeding lines calibrated out through TRL, measured for bias voltages V_{GD} ranging from $0\,\mathrm{V}$ to $-2\,\mathrm{V}$, and shown on Fig. 1, show a very adequate switching, with an insertion loss on the 'ON' state of $1.5\,\mathrm{dB}$, and an increase in transmission loss of up to $6.5\,\mathrm{dB}$ at $28\,\mathrm{GHz}$ in the 'OFF' state, within that biasing range.

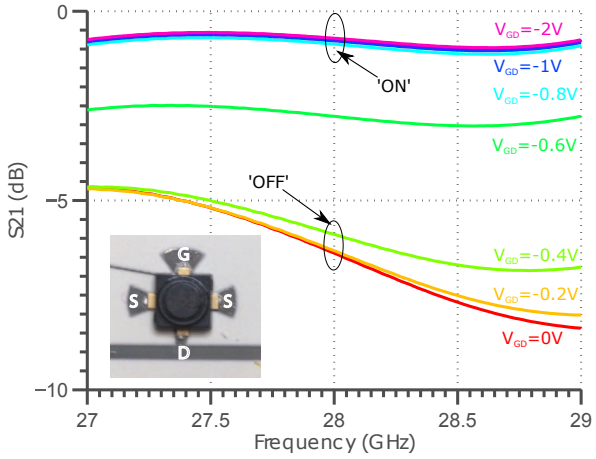

Fig. 1: Measured S_{21} through the switch, for V_{GD} bias voltages ranging from $0\,\mathrm{V}$ to $-2\,\mathrm{V}$, and a picture of the printed switch (inset)

B. Dual-polarized linear antenna array

A dual-polarized linear antenna array, with two ports enabling respectively cross-polarized radiating modes, was designed, printed and tested. The measured results, compared with simulations, are shown on Fig. 2b.

Measurements and simulations are in good agreement, but a degeneracy of the resonance of port 1 is observed in the measurements at $27\,\mathrm{GHz}$, and is attributed to coupling between the resonant-mode of this polarization, and the fine bias feed line added to that port (which can be seen on the top-right corner of the structure on Fig. 2a).

C. Ultra-low-power oscillator circuit and solar cell

In order to encode the identification and sensing information, a low power LMC555 oscillator circuit was implemented,

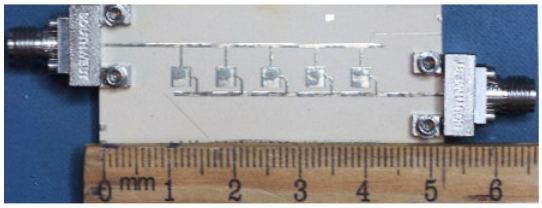

(a)

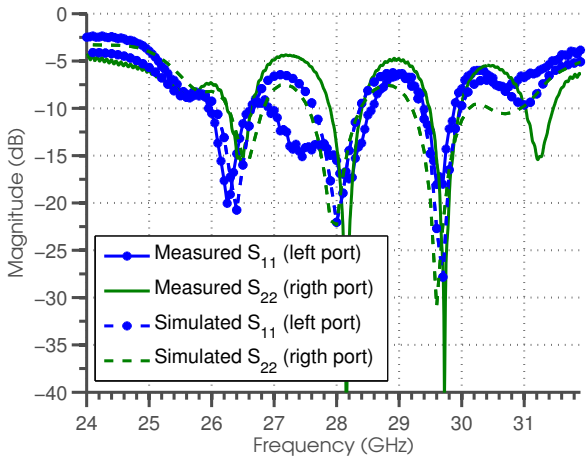

(b)

Fig. 2: (a) Image of the printed linear antenna array and (b) measured and simulated S_{11} and S_{22} of the printed linear antenna array

and its output was used to bias the switches, therefore implementing the driving frequency for the backscatter modulation. The oscillating frequency of this circuit is determined by the value of an RC impedance. Here, the capacitor is set as constant, while the resistor can either be chosen as constant (for identification encoding, for instance) or, as in this system, take the shape of a printed resistometric sensor (as described in Sec. III-D). The circuit was connected to two out of five cells of a MP3-25 flexible solar cell. Under an illumination providing a measured voltage of $1.5\,\mathrm{V}$, an oscillation frequency of $1.4\,\mathrm{MHz}$, and a power consumption of $216\,\mu\mathrm{W}$ were measured.

D. Fully-inkjet-printed CNT-based ammonia sensor

A carbon-nanomaterial-based ammonia sensor was used in the proposed system, in order to enable it with gas sensing capabilities. The sensor was fabricated by first inkjet-printing a custom ink, made by dispersing PABS-functionalized single-wall-carbon-nanotubes (P8-SWNT from Carbon Solutions) in water. Once printed and dried, inter-digitated-electrodes (IDEs) were printed with SNP ink onto the CNT film, in order to interface it. The resistometric component was then tested in a controlled-environment chamber. The results of this characterization (shown on Fig. 3), display a very large sensitivity (defined as the relative resistance change, with reference to the resistance at $t = 0$), with a relative sensitivity

978-1-5090-6360-4/17/$31.00 ©2017 IEEE

of more than 12 % after exposure to 2ppm of ammonia for one hour. The sensor is therefore very much capable of detecting a concentration of 2ppm, which is 25 times smaller than the general OSHA Permissible Exposure Limit (PEL) of 50ppm.

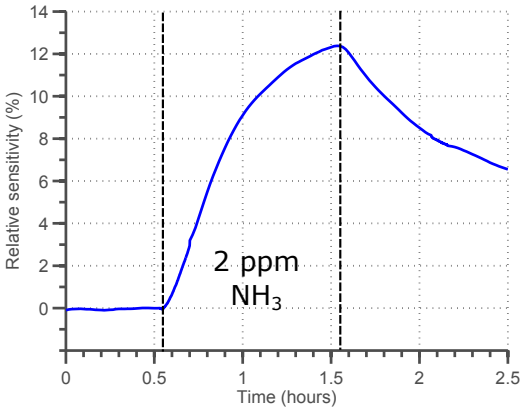

Fig. 3: Measured relative response of a printed SWCNT-PABS-based sensor to 2ppm of ammonia

IV. Printed Van-Atta reflectarray system performance

A. System characterization

After the design steps were completed, resulting in the components reported in Sec. III, the Van-Atta array, including five of the linear antenna arrays described in Sec. III-B, the particular Van-Atta connecting network, and the switches on the lines of this network, were assembled together. The cross-polarized differential monostatic RCS of the structure (shown in Fig. 4) was then measured in an anechoic chamber, using two side-by-side cross-polarized emitting and receiving antennas, at different incidence angles. This was done by controlling the biasing of the switches of the array, and measuring the RCS difference between 'ON' and 'OFF' states.

A 6-inch-radius metal sphere was used as a reference target, for accurate normalization of the RCS measurements. The results of this test, at the measured optimal frequency of $27.978\,\mathrm{GHz}$, are shown on Fig. 5 and display the typical Van-Atta response, with a maximum RCS of $-29\,\mathrm{dBsm}$, and a variation of less than $7\,\mathrm{dB}$ from -50° to 50° of interrogation angle: the structure displays a high and largely isotropic differential RCS.

B. Wireless sensing

The Van-Atta backscatterer was set onto a wall, and wirelessly interrogated at a distance of $5\,\mathrm{m}$ using a custom reader (shown on Fig. 7) whose IF output was measured using a RSA3408A spectrum analyzer. For this test, the array was fed through a power supply, as the indoor lighting conditions were not sufficient in order to provide enough voltage for the system that was optimized for outdoor operation. In this configuration, the sensor was then exposed to a short illumination of pure anhydrous ammonia. The resulting shift in the read backscatter modulation frequency is displayed in the real-time spectrogram of Fig. 6, and shows a quick response of the sensor (and therefore the related backscatter modulating frequency) to the exposure to ammonia, before returning to a stable final state.

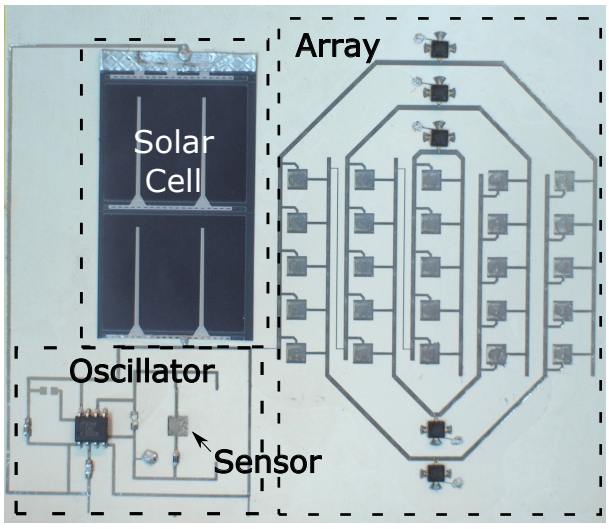

Fig. 4: Assembled printed active Van-Atta reflectarray

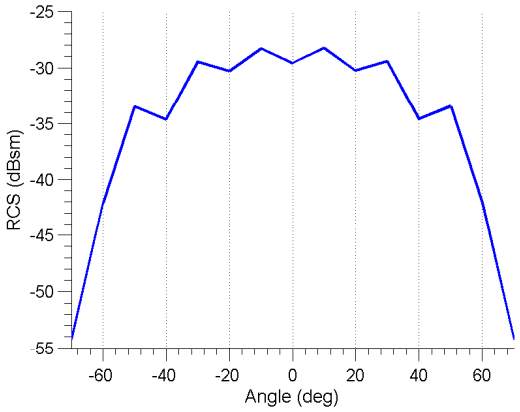

Fig. 5: Measured cross-polarized differential monostatic RCS of the active Van-Atta reflectarray prototype

C. Long range detection

In order to demonstrate its long-range detection capabilities, the proposed backscatter-modulation reflectarray was set onto a shelf, illuminated with an artificial light source with an illuminance of $900\,\mathrm{lx}$ (more than one order of magnitude less than in average outdoor daylight), and interrogated at a distance of $80\,\mathrm{m}$. The emitted power used for the test was on the order of $13\,\mathrm{dBm}$ (with the subtraction of minor cable losses), which was fed to the identical lens antenna system used in [3], yielding an EIRP on the order of $41\,\mathrm{dBm}$. Both emitting and receiving antennas, operating within the same lens antenna system, were cross-polarized. It should be noted that this configuration takes advantage of the rare ability of this

978-1-5090-6360-4/17/$31.00 ©2017 IEEE

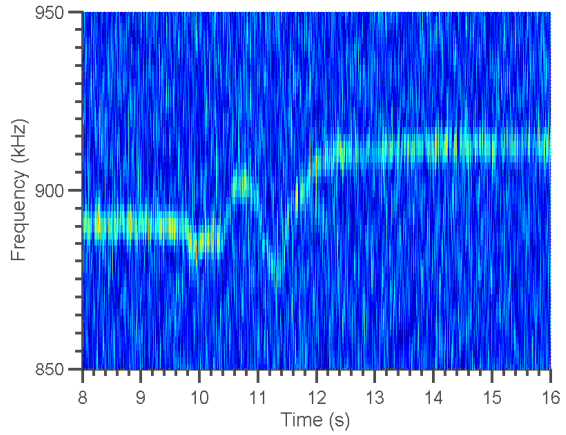

Fig. 6: Real-time spectrogram of the wirelessly-measured response of the printed Van-Atta reflectarray system to exposure to a short illumination of pure anhydrous ammonia

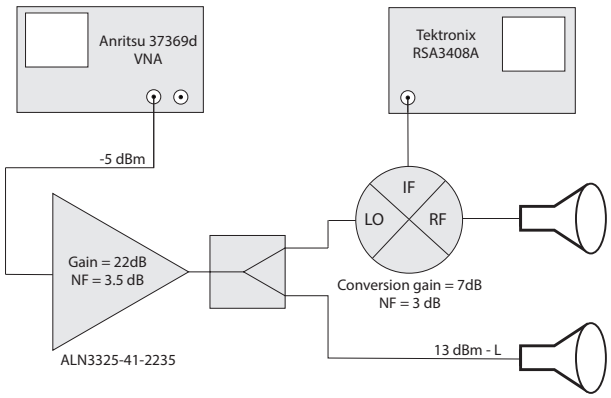

Fig. 7: Schematic of the custom reader used for the long-range detection test

RFID tag to cross-polarize its reflected signal with respect to the CW impinging from the reader, thus enabling improved self-interference rejection through the use of cross-polarized RX and TX reader channels. The measured signal to noise ratio at this distance, with a signal level of $-114\,\mathrm{dBm}$ shown in the measured spectrum in the inset of Fig. 8, was on the order of $4\,\mathrm{dB}$, and was effectively limited by the high phase noise ($-60\,\mathrm{dBc\,Hz^{-1}}$ at $10\,\mathrm{kHz}$ offset and $20\,\mathrm{GHz}$ center frequency) of the output signal of the Anritsu 37369A, used as the local oscillator for the reader system. With the use of state-of-the-art signal generation technology (under $-110\,\mathrm{dBc\,Hz^{-1}}$ phase noise in the same context), and taking advantage of the maximum 5G base-station EIRP of $75\,\mathrm{dBm/100MHz}$, reading ranges in excess of $1\,\mathrm{km}$ could be envisioned.

V. Conclusion

In this work, a novel printed 5G-compatible, energy autonomous, long-range-compatible, printed wireless sensing RFID system was reported. The minimalist approach adopted in this effort was used to introduce a long-range-compatible

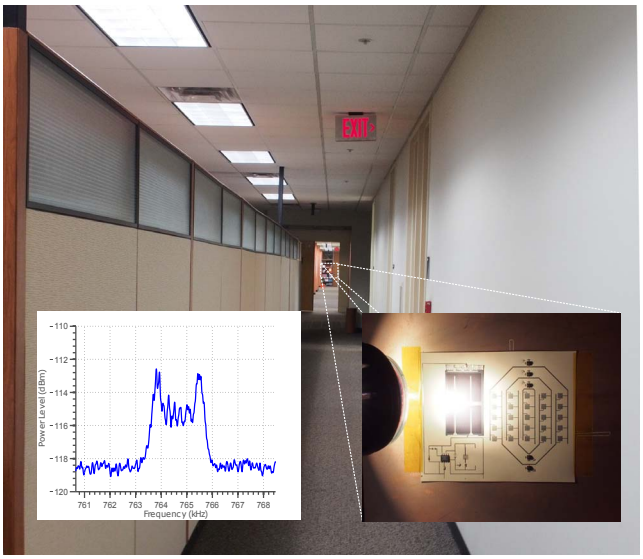

Fig. 8: Long-range ($80\,\mathrm{m}$) measurement configuration of the Van-Atta reflectarray sensor, and the measured IF spectrum (inset)

and energy autonomous sensing system which, along with the rapidly-maturing technologies of fully-printed solar cells [5], and transistors and digital circuits [6], provides the potential for fully-printed low-cost energy-autonomous ultra-long-range RFID sensing systems. Such topologies may thereby set the foundation for the emergence of low-cost mm-wave Smart Skins of the IoT, interfaced at long range through soon-to-be-ubiquitous 5G systems and networks.

Acknowledgment

The authors would like to acknowledge the support of DTRA for this work.

References

[1] J. F. Salmeron, F. Molina-Lopez, A. Rivadeneyra, A. V. Quintero, L. F. Capitan-Vallvey, N. F. de Rooij, J. B. Ozaez, D. Briand, and A. J. Palma, "Design and Development of Sensing RFID Tags on Flexible Foil Compatible With EPC Gen 2," *IEEE Sens. J.*, vol. 14, no. 12, pp. 4361–4371, Dec. 2014.

[2] A. P. Sample, J. Braun, A. Parks, and J. R. Smith, "Photovoltaic enhanced UHF RFID tag antennas for dual purpose energy harvesting," in *2011 IEEE International Conference on RFID*, Apr. 2011, pp. 146–153.

[3] J. G. D. Hester and M. M. Tentzeris, "Inkjet-printed flexible mm-wave Van-Atta reflectarrays: A solution for ultra-long-range dense multi-tag and multi-sensing chipless RFID implementations for IoT Smart Skins," *IEEE Trans. Microw. Theory Tech.*, vol. 57, no. 5, pp. 1303–1309, May 2017.

[4] J. A. Vitaz, A. M. Buerkle, and K. Sarabandi, "Tracking of metallic objects using a retro-reflective array at 26 GHz," *IEEE Trans. Antennas Propag.*, vol. 58, no. 11, pp. 3539–3544, 2010.

[5] T. M. Eggenhuisen, Y. Galagan, A. F. K. V. Biezemans, T. M. W. L. Slaats, W. P. Voorthuijzen, S. Kommeren, S. Shanmugam, J. P. Teunissen, A. Hadipour, W. J. H. Verhees, S. C. Veenstra, M. J. J. Coenen, J. Gilot, R. Andriessen, and W. A. Groen, "High efficiency, fully inkjet printed organic solar cells with freedom of design," *J. Mater. Chem. A Mater. Energy Sustain.*, vol. 3, no. 14, pp. 7255–7262, 2015.

[6] M. Ha, J.-W. T. Seo, P. L. Prabhumirashi, W. Zhang, M. L. Geier, M. J. Renn, C. H. Kim, M. C. Hersam, and C. D. Frisbie, "Aerosol jet printed, low voltage, electrolyte gated carbon nanotube ring oscillators with sub-5 μs stage delays," *Nano Lett.*, vol. 13, no. 3, pp. 954–960, 13 Mar. 2013.

978-1-5090-6360-4/17/$31.00 ©2017 IEEE